Whitcher et al. *NPG Asia Materials* (2020) 12:37
https://doi.org/10.1038/s41427-020-0218-7

NPG Asia Materials

ARTICLE Open Access

Correlated plasmons in the topological insulator Bi_2Se_3 induced by long-range electron correlations

Thomas J. Whitcher[1,2,3], Mathieu G. Silly[4], Ming Yang[5], Pranab Kumar Das[2], David Peyrot[6], Xiao Chi[2,3], Mahmoud Eddrief[7], Jisoo Moon[8], Seongshik Oh[8], Antonio H. Castro-Neto[1,3], Mark B. H. Breese[1,2], Andrew T. S. Wee[1,3], Fabien Silly[6] and Andrivo Rusydi[1,2,3,9,10]

Abstract

Recently, electron correlation has been shown to play an important role in unconventional plasmon generation in highly correlated electron systems. Electrons in topological insulators, on the other hand, are massless and insensitive to nonmagnetic scattering due to their protection by time-reversal symmetry, which makes these materials appealing platforms for hosting exotic plasmonic excitations. Here, using a combination of angle-dependent spectroscopic ellipsometry and angle-resolved photoemission spectroscopy as a function of temperature supported by first-principles calculations, we reveal a new pair of correlated plasmonic excitations at 1.04 and 1.52 eV and a significant Fermi level shift of 0.12 eV accompanied by spectral weight transfer in the topological insulator bismuth selenide (Bi_2Se_3). Interestingly, such a spectral weight transfer over a broad energy range causes a drastic change in the charge carrier density whereby the contribution of charge carriers in the bulk starts to rival those in the surface states and Bi_2Se_3 becomes more uniformly conducting. Our results show the importance of electronic correlations in determining the electronic structure and appearance of correlated plasmons in topological insulators and their potential applications in plasmonics.

Introduction

In recent years, three-dimensional topological insulators have attracted considerable interest due to their fascinating fundamental properties and potential applications arising from their electrically conducting surface but insulating bulk[1–8]. A strong spin-orbit coupling close to the surface inverts the conduction and valence bands, creating a Dirac cone through which charge carriers can be transported[2,9]. Bismuth selenide (Bi_2Se_3) is one of the most commonly investigated topological insulators[5,10,11] alongside bismuth telluride (Bi_2Te_3)[6] and antimony telluride (Sb_2Te_3)[12–14]. In particular, considerable effort has been made to study various types of plasmons that have also been shown to occur in topological insulators[15], including surface[16–18] and Dirac plamons[19–21]. Dyakonov plasmons have also recently been discovered in the optical regime using electron energy-loss spectroscopy and theoretical modeling[22,23]. The potential applications of topological insulators have now begun to be realized in the real world[13,14], including those in quantum computing[3,4], terahertz detectors[24–26], nanomechanics[27,28], crystallization[29], and plasmonic[30], photonic[31,32] and spintronic devices[5–7].

In this study, we focus on Bi_2Se_3 because some of the advantages of this material are that the suppression of Se vacancies favors the stability of Bi_2Se_3-based devices[33,34] and that it can be easily generated as bulk crystals for use in devices by the Bridgman-Stockbarger method[35] and by molecular beam epitaxy[36,37]. Although the electronic properties of Bi_2Se_3 and the other topological insulators have been thoroughly investigated, there has been very limited, if any, study on the electronic correlation and how the electronic correlation influences the electronic structure, in particular as a function of temperature.

Correspondence: Andrivo Rusydi (phyandri@nus.edu.sg) or Thomas J. Whitcher (c2dwtj@nus.edu.sg) or Fabien Silly (fabien.silly@cea.fr)
[1]Department of Physics, National University of Singapore, 2 Science Drive 3, Singapore 117551, Singapore
[2]Singapore Synchrotron Light Source, National University of Singapore, 5 Research Link, Singapore 117603, Singapore
Full list of author information is available at the end of the article

Recently, electronic correlation has been shown to play an important role in unconventional plasmon generation in correlated electron systems[38–42]. This has generated a new idea of studying optical and electronic structures and searching for multiplasmon generation in topological insulators.

Electron spectroscopies, such as angle-resolved photoemission spectroscopy (ARPES), on the one hand, have already been extensively used to study these materials, focusing on the Dirac cone and electronic dispersion closest to the bulk band gap and surface states[43,44]. On the other hand, a direct way to probe the electronic correlation is to measure spectral weight transfer using spectroscopic ellipsometry, which can be used to simultaneously obtain the complex dielectric function and the loss function[38,45,46]. However, until now, no temperature-dependent spectroscopic ellipsometry has been performed on this system, and therefore, our understanding of the electronic correlations is very limited[47,48]. In this article, using a combination of temperature- and angle-dependent spectroscopic ellipsometry and angle-resolved photoelectron spectroscopy (ARPES) supported by first-principles calculations, we reveal that upon cooling, Bi_2Se_3 shows unusual spectral weight transfer over a broad energy range accompanied by the occurrence of a new type of correlated plasmons and a shift in the Fermi level. The complex dielectric and loss functions of the topological insulator are simultaneously determined as a function of temperature, and from these, we deduce that the cause of the temperature-dependent shift is that the long-range electron-electron correlation affects the Fermi level.

Experimental section

Sample preparation

Epitaxial growth of Bi_2Se_3 thin films on 5×5 mm^2 GaAs (111) substrates was performed using an MBE reactor, where source fluxes were provided by conventional standard effusion cells. Epitaxial growth of Bi_2Se_3 epilayers was then carried out at $T = 300$ °C with a Se/Bi beam equivalent pressure ratio greater than 6.5. The Bi_2Se_3 thin films are composed of many micron-sized grains covering the whole substrate. Samples were capped with protective amorphous Se layers to prevent contamination and oxidation prior to air exposure, depending on the kind of measurement planned.

Angle-resolved photoemission spectroscopy

For angle-resolved photoemission spectroscopy, a specific procedure implying the use of a Se cap layer was used, allowing us to recover a clean surface under UHV after a mild annealing step (with a pressure not exceeding 5×10^{-10} mbar). ARPES measurements were carried out using a high-resolution Scienta SES 2002 photoelectron energy analyzer equipped with a delay line detector at the TEMPO beamline of Synchrotron SOLEIL[49] and a high-resolution Scienta DA30 electron analyzer equipped with a 3-dimensional spin detector at the SUV Beamline of the Singapore Synchrotron Light Source[50]. The beam diameter for ARPES in both cases was on the order of a few hundred μm^2. This is much smaller than the sample surface, and therefore, the signal is from the thin film.

Spectroscopic ellipsometry

Spectroscopic ellipsometry measurements were carried out using a variable-angle spectroscopic ellipsometer (V-VASE, J. A. Woollam Co.) with a rotating analyzer and a compensator at the Singapore Synchrotron Light Source (SSLS). The measurements were taken in the energy range of 0.6−6.0 eV while the sample was inside a UHV cryostat with a base pressure of 10^{-8} mbar. The sample was heated to 475 K and annealed for 12 h to remove the α-Se cap. The measurements were taken at angles of 68°, 70° and 72°, which are limited in range by the UHV windows. Measurements were taken over a range of temperatures from 77 K to 475 K at an angle of 70°. The stabilization accuracy of the temperature was ±0.5 K, and the sample was cooled/heated slowly and evenly across the sample. When at the target temperature, the sample was left to stabilize for 10 min. Each measurement at the specified temperature took approximately 2 h to complete. The output data, ψ and Δ, are shown in Supplementary Fig. S1. Analysis of the spectroscopic ellipsometry data was performed using the W-VASE analysis program, where the complex dielectric function was obtained using a fitting procedure that models the data and takes into account the anisotropy of the sample[51]. Further details are provided in the Supplementary Material.

First-principles calculations

First-principles calculations were performed within the framework of density-functional theory (DFT) using the generalized gradient approximation (GGA) based on the Perdew-Burke Ernzerhof (PBE) functional and projector augmented wave (PAW) potentials, as implemented in the Vienna ab initio Simulation Package (VASP5.4.4.18)[52,53]. The cutoff energy for the plane wave expansion was set to 500 eV. In all the calculations, spin-orbital interactions were included, and the criterion of electronic convergence was set to 1.0×10^{-6} e. The experimental lattice constants ($a = b = 4.14$ Å and $c = 28.64$ Å) of the Bi_2Se_3 crystal were adopted, in which the atoms were optimized until the force was less than 0.01 eV/Å, including the van der Waals correction (DFT-D3)[54]. A Γ-centered $6 \times 6 \times 6$ k-point mesh was used to sample the first Brillouin zone (BZ) of the Bi_2Se_3 primitive cell.

Results and discussion

Figure 1a, b show the real, ε_1, and imaginary, ε_2, parts of the complex dielectric function, respectively, measured using spectroscopic ellipsometry over a range of

temperatures from 475 K down to 77 K. There is a clear difference in both parts of the dielectric function as Bi_2Se_3 is cooled, with the largest changes occurring at and around 2.0 eV. There is also an edge that occurs in the ε_2 spectra at 1.0 eV for all temperatures that becomes sharper as the sample is cooled. As Bi_2Se_3 is a topological insulator, the electronic structure is highly dependent on the thickness of the sample. Fortunately, another advantage of spectroscopic ellipsometry is that we can use this technique to simultaneously measure the thickness of Bi_2Se_3, and in this case, it is 30.2 nm (or 29 quintuple layers), which is also later confirmed by atomic force microscopy (AFM) measurements.

Since spectroscopic ellipsometry is a photon-in photon-out technique, it can be used to search for plasmonic activity in correlated electron systems[41,55]. For sub-X-ray photons, the momentum transfer, q, is finite but approaches zero because it is much less than the crystal momentum. In this limit, the distinction between the longitudinal and transverse $\varepsilon(\omega)$ vanishes, i.e.,

$$lim_{q\to 0} e_l(q,w) = etqw \tag{1}$$

which allows sub-X-ray spectroscopic ellipsometry to probe both optical and plasmonic properties of materials in the low-q limit[43,44]. Figure 1c shows a comparison of ε_2 and the loss function given by

$$LF = -Im(1/e) = -Im(1/(e_1 + ie_2)) \tag{2}$$

for all temperatures measured between 475 and 77 K in the spectral region of 0.6–0.6 eV. The peaks in the loss function at 1.04 and 1.52 eV indicate the presence of a plasmon at these energies below 250 K, and they are closely linked to the peaks in ε_2 at 1.00 and 1.48 eV, which are optical excitations. These peaks are identified by fitting the data to a Gaussian-Lorentzian model and applying background subtraction to reveal the positions of the peaks, as shown in Supplementary Fig. S2.

The existence of both peaks within 40 meV of the peaks in ε_2 means that there is a strong coupling between the optical and plasmonic excitations of Bi_2Se_3 and is indicative of correlated plasmons[38,39]. The correlated plasmons appear in both the ε_2 and loss function spectra, which means that the correlated plasmons can readily be excited by, decay radiatively into and thus couple with free space photons without any external mechanisms. This is one of the specific properties that identify the peaks in the loss function as corresponding to correlated plasmons. The other properties are as follows. First, unlike conventional plasmons, correlated plasmons occur in materials with a low free charge density, such as the bulk of Bi_2Se_3 so do not arise from the collective oscillation of free charges but from the collective oscillation of quasi-local (or correlated) electrons[38,39]. This is directly linked to the second property in that they therefore have more than one plasmon energy, in this case at 1.04 and 1.52 eV. The energies of the correlated plasmons are determined not only by the charge carrier density of the free electrons but also by the potential energy of the long-range correlation between electrons. As there are multiple long-range correlations present between quasi-local electrons, there can be multiple correlated plasmon energies. Finally, correlated plasmons also have a significantly lower loss than conventional plasmons and a positive real part of the dielectric function, ε_1, both of which can be seen in Fig. 1[38,39]. The limit for observable correlated plasmons in $Sr_{1-x}NbO_{3+d}$ is 20 nm; while this may be different between materials, we are still able to observe correlated plasmons in a 30 nm thin film of Bi_2Se_3[38,39].

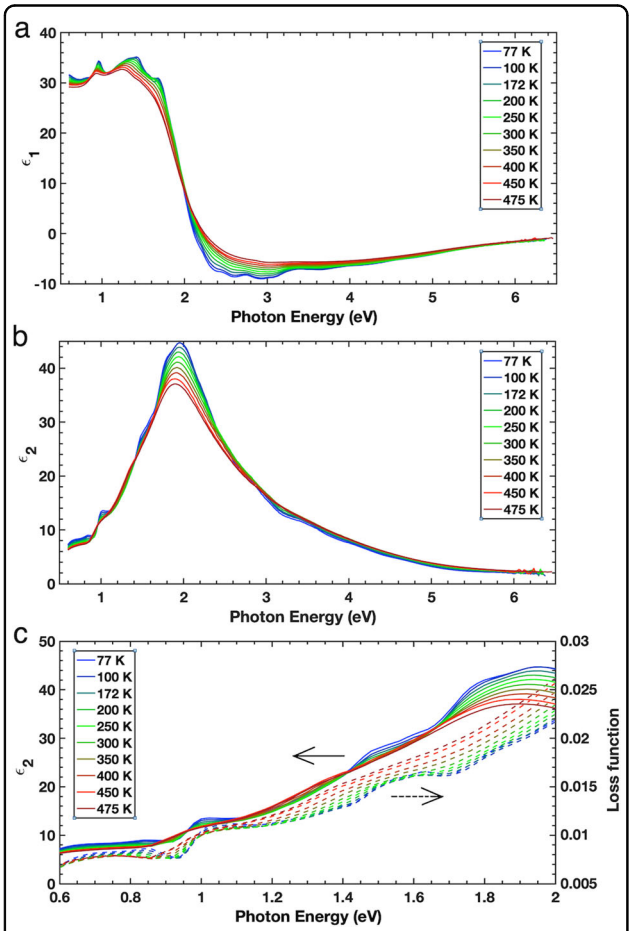

Fig. 1 Complex dielectric function and loss function of Bi_2Se_3. a Real and **b** imaginary parts of the dielectric function of Bi_2Se_3 modeled from spectroscopic ellipsometry data as a function of temperature. **c** Comparison of the imaginary part of the dielectric function, ε_2 (solid line), and the loss function Im(-1/ε) (dashed line) for all temperatures.

Although a plasmonic resonance has been detected in another topological insulator, $Bi_{1.5}Sb_{0.5}Te_{1.8}Se_{1.2}$, within the optical–UV range[56], this is the first time that correlated plasmons have been detected in topological insulators. We note that high-energy plasmonic resonances have been detected in Bi_2Se_3 above 7 eV using energy −loss spectroscopy and scanning transmission electron microscopy (STEM)[57].

The difference in the complex dielectric function with temperature (shown in Supplementary Fig. 1) highlights the increasing change that can be seen in the topological insulator's electronic response to external electromagnetic fields with temperature. There is a significant shift in the spectral weight of ε_2 as Bi_2Se_3 is cooled, and to explore this, we need to look at the optical conductance, which is related to ε_2 by

$$s_1 = we_2/4p \tag{3}$$

where ω is the photon frequency and σ_1 is the real part of the complex conductivity.

Figure 2a shows the optical conductivity of the Bi_2Se_3 thin film for each of the temperatures measured. For the spectral weight transfer analysis, the conductivity was divided into three spectral regions as follows: I: 0.60–1.65 eV, II: 1.65–2.90 eV and III: 2.90–6.00 eV. Figure 2b shows the change in the conductivity in region III as the sample is cooled from 475 K to each of the measured temperatures, and there is a clear and consistent decrease in the spectral weight starting from 250 K down to 77 K. This is converse to what is seen in region II of Fig. 2a, where the spectral weight appears to increase. The integration of the optical conductivity is related to the free charge carrier density, n_e, via the charge conserving *f*-sum rule:

$$\int_0^\infty \sigma_1(\omega)d\omega = \pi n_e e^2/2m_e \tag{4}$$

where e is the elementary charge and m_e is the electron mass[38,45,51,58]. Therefore, the integration of the part of the spectral region between E_1 and E_2, given by

$$W = \int_{E1}^{E2} \sigma_1(E)dE \tag{5}$$

is proportional to the number of free charge carriers within that spectral region. By analyzing the change in W with temperature, we can gain insight into the behavior of the free charge carriers as the Bi_2Se_3 sample is cooled[38,45,58].

The total spectral weight, W, of the Bi_2Se_3 thin film across the measured spectral range of 0.6–6.0 eV is shown

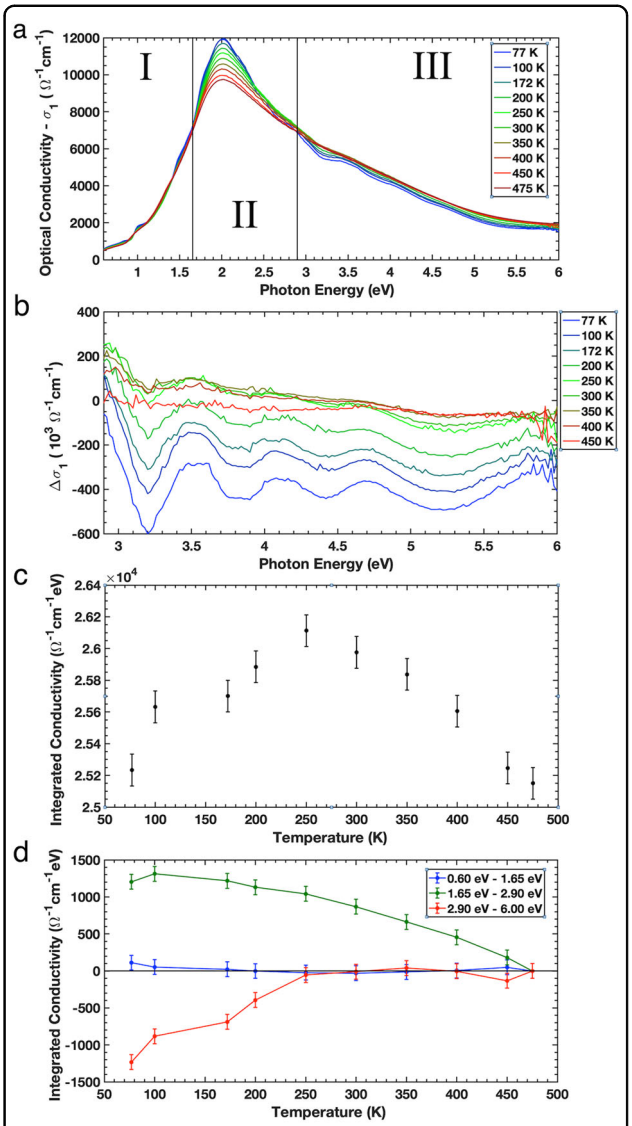

Fig. 2 Optical conductivity of Bi_2Se_3. a Optical conductivity of Bi_2Se_3 as a function of temperature divided into three spectral regions. **b** Difference in the optical conductivity between 475 K and the colder measurements in the third region between 2.9 and 6.0 eV. **c** Optical conductivity of Bi_2Se_3 integrated over the whole spectrum as a function of temperature. **d** Change in the integrated optical conductivity of the three different spectral regions as the sample is cooled from 475 K.

in Fig. 2c as a function of temperature. There is an increase in W as the sample is cooled from 475 to 250 K, followed by a decrease down to roughly the same level as that at 475 K as the sample is further cooled to 77 K. This result indicates that there are more electrons with energies between 0.6 and 6.0 eV at 250 K than at any other temperature. This means that above and below 250 K, the number of electrons with energies outside of the spectral range measured is increasing. This shift in spectral weight cannot be explained by thermal activation, as the energies

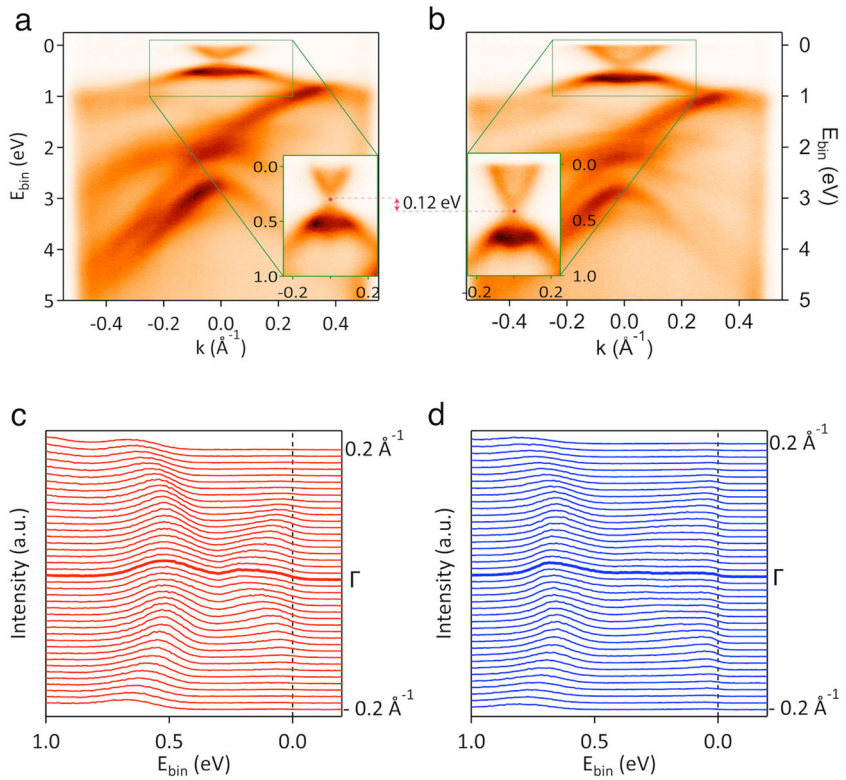

Fig. 3 ARPES measurements of Bi_2Se_3. a, **b** Electronic band dispersion of Bi_2Se_3 thin film measured using a 60 eV photon energy along the Γ-M direction at 300 K and 100 K, respectively. **c**, **d** The energy dispersion curves of the spectra shown in the panel **a** and **b** insets, respectively. The energies are measured relative to the Fermi energy.

associated with temperatures below 500 K are too small (<43 meV); therefore, the extra energy gained or lost must come from the potential energy electron-electron correlations. Both of the correlated plasmons seen in Fig. 1c disappear at temperatures of 250 K and above, which also coincides with the drop in electron conductivity and thus electron density seen in Fig. 2c.

Figure 2d shows the change in *W* for each of the three spectral regions from Fig. 2a as the sample is cooled from 475 K to 77 K. While there is little change in the low-energy and mid-energy regions below 250 K, the loss in the spectral weight in the high-energy region represents a significant shift in the electron density from this spectral range to higher energies (above 6.0 eV). The increase in electron energy on the order of several eV comes from the long-range electron-electron correlations, which are now prominent due to decreased electronic screening[38]. This in turn gives rise to plasmonic activity, which has been seen in conductive materials[38,45,59].

One of the important effects of the appearance of high-energy plasmons is that electron scattering may be able to occur within the system. The scattering of free charge carriers in the surface states of topological insulators is extremely limited, as back-scattering from nonmagnetic impurities is prohibited by time-reversal symmetry[2], phonons are too weak for electron scattering[60] and the conventional Dirac plasmons reported in the surface states have energies in the THz regime (on the order of 10 meV) and thus cannot cause significant scattering[20]. However, since the correlated plasmons have energies on the order of 1 eV, they can cause electron scattering from the surface states to the bulk, as seen in other 2D materials such as graphene[61]. To determine if this is the case, we use ARPES to detect changes in the Fermi level as a function of temperature.

Figure 3 presents the electronic band structure of the Bi_2Se_3 thin film along the Γ-M direction measured using ARPES with an incident photon energy of 60 eV. Panel (a) shows the spectrum taken at room temperature (300 K), while panel (b) shows the spectrum taken at liquid nitrogen temperature (100 K). The Dirac fermion surface state is clearly observed at both room temperature and low temperature. Other band features at lower binding energies are also very sharp, indicating the good quality surface of our thin film. The most striking change in the low temperature spectrum compared to the room temperature spectrum is the location of the Dirac point. The Dirac point at room temperature is observed at a binding

energy of 0.30 eV, while the Dirac point has shifted to the higher binding energy of 0.42 eV at 100 K (the energies are measured with respect to the Fermi energy). At lower temperatures, the shift in the Dirac point by 0.12 eV towards a higher binding energy shows that the electronic structure of the Bi_2Se_3 film has changed. Although initial charge transfer might occur between the substrate and thin film, this does not affect the changes in the electronic structure measured as a function of temperature[62].

Although surface effects such as residual moisture contamination in the vacuum chamber[63] and subsequent deselenization can also alter the electronic structure, in the time frame of the measurements, these effects are minimized (see the Supplementary Material for further details). One possible mechanism that might occur is charge build-up in the GaAs substrate due to the substrate's pyroelectric properties[64,65]; however, this is minimized by the slow heating/cooling of the sample. The substrate is also grounded, and the sample is given time to stabilize at the required temperature. The measurements at a given temperature take approximately 2 h to complete, so any charge build-up within the substrate would most certainly dissipate over time. Another possible mechanism is the effect of the GaAs substrate band gap, where photons with energies higher than it may charge the substrate. However, because the energy gap for GaAs is 1.45 eV, the films cannot be charged because there is no state below the band gap of GaAs. Furthermore, above 1.45 eV, the photon penetration depth dramatically drops and only reaches 0.03 microns (30 nm) in the film; therefore, the signal only comes from the film (Supplementary Fig. 2). All these results clarify that the correlated plasmons are truly intrinsic properties of Bi_2Se_3 and not from other effects, such as the substrate.

The shift in the spectrum can also be seen in the energy distribution curves (EDCs), as shown in panels (c) and (d) of Fig. 3. Apart from the downward shift in the spectra, the spectral features of Bi_2Se_3 at low and high temperatures are similar. This suggests an increase in n-doping[66], which would have profound effects on the surface and transport properties of the material[43]. The consequences of this shall now be explored in terms of carrier contributions from the bulk and surface states.

The free charge carrier densities of both the bulk and surface states can be calculated from the optical conductivity in Fig. 2 and the charge carrier mobility by using the following equation:

$$\sigma = n_e e \mu_e \tag{6}$$

where μ_e is the electron mobility. The electron mobility of Bi_2Se_3 is given as 880 cm^2/Vs at room temperature and 1380 cm^2/Vs at low temperatures in ref. 5. From this, the electron density is calculated to be $1.83 \times 10^{20}\,cm^{-3}$ at room temperature and $1.15 \times 10^{20}\,cm^{-3}$ at 100 K, with a decrease of $6.8 \times 10^{19}\,cm^{-3}$ as the sample is cooled.

The ARPES images in Fig. 3 at 300 and 100 K show that although the Fermi level with respect to the Dirac point has increased at 100 K, there are actually fewer free carriers within the measured spectral range up to 6.0 eV than there are at 300 K. This matches what is shown in Fig. 2a. We can also use the energy of the conduction band minimum from Figs. 3a and 3b to calculate the charge density in the conduction band within the bulk of Bi_2Se_3 using the following equation:[67,68]

$$E_{CB} = \hbar^2/2m^* \left(3\pi^2 n_{BD}\right)^{2/3} \tag{7}$$

where n_{BD} is the bulk carrier density, m^* is the effective electron mass, which is usually ≈0.15m_e in Bi_2Se_3, and E_{CB} is the difference between the Fermi energy and the conduction band minimum. For 100 K, E_{CB} is 330 meV, which gives a bulk carrier density of $5.00 \times 10^{19}\,cm^{-3}$, and for 300 K, E_{CB} is 220 meV, which yields a bulk carrier density of $2.72 \times 10^{19}\,cm^{-3}$. Note that these values are very high for what is supposed to be an insulating bulk, but in reality, few Bi_2Se_3 samples created achieve a truly insulating bulk due to the Mott criterion and Ioffe-Regel criterion[67]. The bulk states can be considered as a bad conductor in most cases or more accurately as a weaker conductor than the surface states. We also note that both the bulk and surface carrier densities in our thin film extracted from the room temperature measurements are similar to those found in Sample B of ref. 69.

The electron densities calculated from ARPES are smaller than those calculated from the spectroscopic ellipsometry data because the values from the latter are the electron densities for the entire sample—both the bulk states and the conducting surface states. Therefore, with these values, we can calculate the percentage of carriers from the surface states that contribute to the overall conduction for each temperature. At 300 K, approximately 85% of carriers come from the surface states, whereas at 100 K, only 57% of the carriers come from the surface states. This result agrees with our earlier hypothesis that the introduction of high-energy correlated plasmons below 250 K would cause electron scattering from the surface to bulk states. However, the n_e calculated from ellipsometry may be underestimated because the spectral range shown in Figs. 2 and 3 is from 0.6 to 6.0 eV, so electrons outside of this energy range are not considered; therefore, the fraction of charge carriers from the surface states at both temperatures may be higher.

Figure 4 shows the first-principles-calculated band structures of Bi_2Se_3 surface slabs near the Fermi level. Figure 4b, c show the undoped case and the n-doped case, respectively, where 0.12 electrons have been artificially added to Bi_2Se_3 in the n-doped case. Details of the calculations are

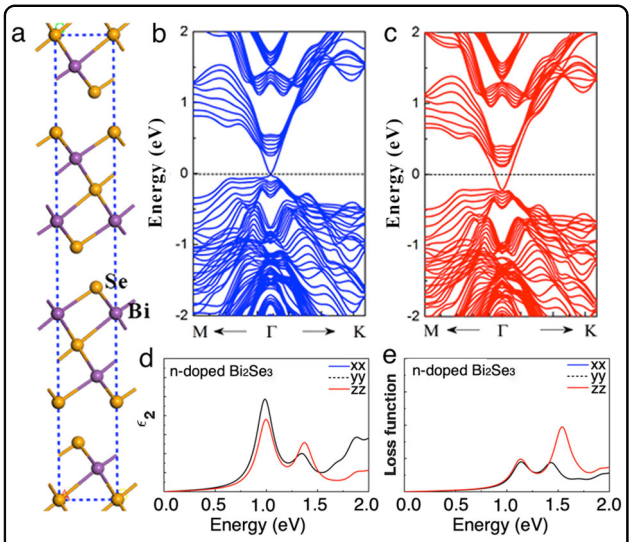

Fig. 4 First-principles calculations of Bi_2Se_3. a Atomistic structure of Bi_2Se_3 (side view). Band structure of Bi_2Se_3 slabs **b** without doping and **c** with 0.12 electron doping. Calculated imaginary dielectric function **d** and loss function **e** of the Bi_2Se_3 primitive cell with electron doping. The contributions of the xx and yy components are equal in both cases.

given in the Supplementary Material[52–54,70–72]. The two simulations show very little change with respect to each other apart from the obvious shift in the Fermi level. The band structures shown in Fig. 4 exhibit a remarkable similarity to the ARPES data in Fig. 3, in which the n-doped simulations and the 100 K data both have a higher Fermi level compared with the high temperature/undoped results. The major difference is that the simulations for undoped Bi_2Se_3 show the Fermi level at the Dirac point, whereas the room temperature ARPES results show the Fermi level to be 0.29 eV above the Dirac point. This difference occurs because the sample is not a perfect Bi_2Se_3 single crystal but a polycrystalline thin film, and as discussed in the Supplementary Material, effects such as moisture contamination (Supplementary Fig. 3a) and deselenization will also shift the Fermi level[73,74]; however, the changes due to temperature are shown to be reversible (Supplementary Fig. 3b).

The calculated optical spectra of Bi_2Se_3 with electron doping are shown in Fig. 4d, e, in which the electron-electron correlation effects were included at the G_0W_0-RPA level. The contributions of p_x and p_y to the dielectric function and loss function are equal, which is why the blue lines of the *xx* component and dashed black lines of the *yy* component overlap in both Fig. 4d, e. Two peaks are found at the energy positions of 1.02 and 1.38 eV in the imaginary part of the dielectric function and electron energy loss function, which we believe are plasmon peaks because they are only due to electron-electron interactions. Together, these plasmons could contribute to the shift in the conduction carrier density from the surface to the bulk through electron scattering.

Because electronic correlation is important for the generation of correlated plasmons, one may consider applying correlated plasmons as a gating material in submicron devices and using temperature to control the on and off states. As Bi_2Se_3 is insulating within the bulk at room temperature, this would keep the device in the 'off' position. When the temperature is lowered, correlated plasmons appear, and the bulk of the material starts to become conducting, which would allow currents to pass through; thus, the device would be in the 'on' position.

Conclusions

In summary, by simultaneously determining the complex dielectric function, loss function and electronic structure and dispersion of Bi_2Se_3 as a function of temperature using a combination of spectroscopic ellipsometry and ARPES supported by theoretical calculations, we observe unusual spectral weight transfer yielding a significant shift in the Fermi level and two correlated plasmons, a new type of plasmons seen in correlated systems. From the spectral weight transfer analysis, we find that upon cooling below 250 K, the decrease in electronic screening leads to an increase in long-range electron correlations, which increase the potential energy of the system and result in the formation of correlated plasmons. Electron scattering from the high-energy correlated plasmons results in an increase in the bulk carrier density and, subsequently, a reversible shift in the Fermi energy. Our results show new correlated plasmons in Bi_2Se_3, and the methodology introduced here can be used to probe plasmons in topological insulators.

Acknowledgements

We thank Z. Li, E. Chew, H. Miao, W. Wong, W. Zaw, C Lim and T.C. Asmara for technical support. This work is supported by Singapore Ministry of Education AcRF Tier-2 (MOE2017-T2-1-135, MOE2018-T2-2-117, and MOE2019-T2-1-163), MOE-AcRF Tier-1 (R-144-000-423-114, R-144-000-398-114, R-144-000-379-114 and R-144-000-368-112), the Singapore National Research Foundation under its Competitive Research Funding (No. R-398-000-087-281), and the 2015 PHC Merlion Project. The authors would also like to acknowledge the Singapore Synchrotron Light Source (SSLS) for providing the facility necessary for conducting the research. The Laboratory is a National Research Infrastructure under the National Research Foundation Singapore. The Centre for Advanced 2D Materials at the National University of Singapore is acknowledged for providing the computing resources. T.J.W., M.S. and M.Y. contributed equally to this work.

Author details

[1]Department of Physics, National University of Singapore, 2 Science Drive 3, Singapore 117551, Singapore. [2]Singapore Synchrotron Light Source, National University of Singapore, 5 Research Link, Singapore 117603, Singapore. [3]Centre for Advanced 2D Materials, National University of Singapore, 6 Science Drive 2, Singapore 117546, Singapore. [4]Synchrotron SOLEIL, L'orme des merisiers, Saint-Aubin, BP 48, 91192 Gif-surYvette, Paris, France. [5]Institute of Materials Research and Engineering, A*STAR, 2 Fusionopolis Way, Singapore 138634, Singapore. [6]Université Paris-Saclay, CEA, CNRS, SPEC, TITANS, F-91191 Gif sur Yvette, Paris, France. [7]Sorbonne Universites, UPMC Univ. Paris 6, CNRS, Institut des NanoSciences de Paris, 4 place Jussieu, 75005 Paris, France. [8]Department of

Physics & Astronomy, Rutgers, The State University of New Jersey, 136 Frelinghuysen Road, Piscataway, NJ 08854, USA. [9]NUSSNI-NanoCore, National University of Singapore, Singapore 117576, Singapore. [10]NUS Graduate School for Integrative Sciences and Engineering, Singapore 117456, Singapore

Author contributions

T.J.W., X.C. and A.R. performed spectroscopic ellipsometry measurements and analysis. M.G.S, D.P., M.E., J.M. and S.O. grew and prepared samples. M.G.S., P.K.D., F.S, D.P. and A.R. performed ARPES measurements and analysis. Y.M., P.K.D., T.J.W. and A.R. performed theoretical calculations and analysis of optical spectra. T.J.W., P.K.D. and A.R. comprehensively analyzed all data and wrote the paper with input from M.E., A.C.-N., M.B., A.T.S.W. and all other coauthors. A.R., M.G.S. and F.S. initiated and led the project.

Conflict of interest

The authors declare that they have no conflict of interest.

Publisher's note

Springer Nature remains neutral with regard to jurisdictional claims in published maps and institutional affiliations.

Supplementary information is available for this paper at https://doi.org/10.1038/s41427-020-0218-7.

Received: 9 August 2019 Revised: 6 November 2019 Accepted: 11 November 2019.
Published online: 29 May 2020

References

1. Hasan, M. Z. & Kane, C. L. Colloquium: topological insulators. *Rev. Mod. Phys.* **82**, 3045 (2010).
2. Fu, L. & Kane, C. L. Topological insulators with inversion symmetry. *Phys. Rev. B* **76**, 045302 (2007).
3. Collins, G. P. Computing with quantum knots. *Sci. Am.* **294**, 57 (2006).
4. Kitaev, A. & Preskill, J. Topological entanglement entropy. *Phys. Rev. Lett.* **96**, 110404 (2006).
5. Zhang, Y. et al. Crossover of the three-dimensional topological insulator Bi2Se3 to the two-dimensional limit. *Nat. Phys.* **6**, 584 (2010).
6. Chen, Y. et al. Experimental realization of a three-dimensional topological insulator, Bi2Te3. *Science* **325**, 178 (2009).
7. Yazyev, O. V., Moore, J. E. & Louie, S. G. Spin polarization and transport of surface states in the topological insulators $Bi_2Se_3$and Bi_2Te_3 from first principles. *Phys. Rev. Lett.* **105**, 266806 (2010).
8. Rechtsman, M. C. et al. Photonic Floquet topological insulators. *Nature* **496**, 196 (2013).
9. Hsieh, D. et al. Observation of time-reversal-protected single-Dirac-cone topological-insulator states in Bi_2Te_3 and Sb_2Te_3. *Phys. Rev. Lett.* **103**, 146401 (2009).
10. Atuchin, V. V. et al. Formation of inert Bi_2Se_3(0001) cleaved surface. *Cryst. Growth Des.* **11**, 5507 (2011).
11. Cheng, P. et al. Landau quantization of topological surface states in Bi_2Se_3. *Phys. Rev. Lett.* **105**, 076801 (2010).
12. Jiang, Y. et al. Landau quantization and the thickness limit of topological insulator thin films of Sb_2Te_3. *Phys. Rev. Lett.* **108**, 016401 (2012).
13. Nechaev, I. A. et al. Quasiparticle spectrum and plasmonic excitations in the topological insulator Sb_2Te_3. *Phys. Rev. B* **91**, 245123 (2015).
14. Pauly, C. et al. Probing two topological surface bands of Sb_2Te_3 by spin-polarized photoemission spectroscopy. *Phys. Rev. B* **86**, 235106 (2012).
15. Politano, A., Lamuta, C. & Chiarello, G. Cutting a Gordian Knot: dispersion of plasmonic modes in Bi_2Se_3 topological insulator. *Appl. Phys. Lett.* **110**, 211601 (2017).
16. Karch, A. Surface plasmons and topological insulators. *Phys. Rev. B* **83**, 245432 (2011).
17. Lai, Y. P., Lin, I. T., Wu, K. H. & Liu, J. M. Plasmonics in topological insulators. *Nanomater. Nanotech.* **4**, 13 (2014).
18. Kogar, A. et al. Surface collective modes in the topological insulators Bi_2Se_3 and $Bi_{0.5}Sb_{1.5}Te_{3-x}Se_x$. *Phys. Rev. Lett.* **115**, 257402 (2015).
19. Politano, A. et al. Interplay of surface and Dirac plasmons in topological insulators: the case of Bi_2Se_3. *Phys. Rev. Lett.* **115**, 216802 (2015).
20. Di Pietro, P. et al. Observation of Dirac plasmons in a topological insulator. *Nat. Nanotech.* **8**, 556 (2013).
21. Stauber, T. Plasmonics in Dirac systems: from graphene to topological insulators. *J. Phys. Condens. Matter* **26**, 123201 (2014).
22. Talebi, N. et al. Wedge Dyakonov waves and Dyakonov plasmons in topological insulator Bi2Se3 probed by electron beams. *ACS Nano* **10**, 6988 (2016).
23. Politano, A., Chiarello, G. & Spinella, C. Plasmon spectroscopy of graphene and other two-dimensional materials with transmission electron microscopy. *Mater. Sci. Semicond. Process* **65**, 88 (2017).
24. Zhang, X., Wang, J. & Zhang, S.-C. Topological insulators for high-performance terahertz to infrared applications. *Phys. Rev. B* **82**, 245107 (2010).
25. Tang, W. et al. Ultrasensitive room-temperature terahertz direct detection based on a bismuth selenide topological insulator. *Adv. Funct. Mater.* **28**, 1801786 (2018).
26. Viti, L. et al. Plasma-wave terahertz detection mediated by topological insulators surface states. *Nano Lett.* **16**, 80 (2016).
27. Lamuta, C. et al. Mechanical properties of Bi_2Te_3 topological insulator investigated by density functional theory and nanoindentation. *Scr. Mater.* **121**, 50 (2016).
28. Lamuta, C. et al. Indentation fracture toughness of single-crystal Bi_2Te_3 topological insulators. *Nano Res.* **9**, 1032 (2016).
29. Macedonio, F., Politano, A., Drioli, E. & Gugliuzza, A. Bi_2Se_3-assisted membrane crystallization. *Mater. Horiz.* **5**, 912 (2018).
30. Politano, A., Viti, L. & Vitiello, M. S. Optoelectronic devices, plasmonics, and photonics with topological insulators. *APL Mater.* **5**, 035504 (2017).
31. Lu, L., Joannopoulos, J. D. & Soljačić, M. Topological photonics. *Nat. Photon.* **8**, 821 (2014).
32. Khanikaev, A. B. et al. Photonic Topological Insulators. *Nat. Mater.* **12**, 233 (2013).
33. Politano, A. et al. Exploring the surface chemical reactivity of single crystals of binary and ternary bismuth chalcogenides. *J. Phys. Chem. C.* **118**, 21517 (2014).
34. Politano, A., Vitiello, M. S., Viti, L., Boukhvalov, D. W. & Chiarello, G. The role of surface chemical reactivity in the stability of electronic nanodevices based on two-dimensional materials "beyond graphene" and topological insulators. *FlatChem* **1**, 60 (2017).
35. Lamuta, C. et al. Nanoindentation of single-crystal Bi_2Te_3 topological insulators grown with the Bridgman–Stockbarger method. *Phys. Status Solidi b* **253**, 1082 (2016).
36. Tabor, P., Keenan, C., Urazhdin, S. & Lederman, D. Molecular beam epitaxy and characterization of thin Bi_2Se_3 films on Al_2O_3 (110). *Appl. Phys. Lett.* **99**, 013111 (2011).
37. Wang, Z. Y., Li, H. D., Guo, X., Ho, W. K. & Xie, M. H. Growth characteristics of topological insulator Bi_2Se_3 films on different substrates. *J. Cryst. Growth* **334**, 96 (2011).
38. Asmara, T. C. et al. Large spectral weight transfer in optical conductivity of $SrTiO_3$ induced by intrinsic vacancies. *J. Appl. Phys.* **115**, 213706 (2014).
39. Van Loon, E. G. C. P., Hafermann, H., Lichtenstein, A. I., Rubtsov, A. N. & Katsnelson, M. I. Plasmons in strongly correlated systems: spectral weight transfer and renormalized dispersion. *Phys. Rev. Lett.* **113**, 246407 (2014).
40. Zhu, T. et al. Generation of multiple plasmons in strontium niobates mediated by local field effects. *Phys. Rev. B* **98**, 235115 (2018).
41. Chaudhuri, A. et al. Quasilocal plasmons in the insulator-metal transition in the Mott-type perovskites $Eu_{0.3}Ba_{0.7}Ti_{1-x}Nb_xO_3$. *Phys. Rev. B* **98**, 165303 (2018).
42. Jia, X. et al. Anomalous acoustic plasmon mode from topologically protected states. *Phys. Rev. Lett.* **119**, 136805 (2017).
43. Green, A. J. et al. Surface oxidation of the topological insulator Bi_2Se_3. *J. Vac. Sci. Tech. A: Vac. Surf. Film.* **34**, 061403 (2016).
44. Hirahara, T. et al. Anomalous transport in an n-type topological insulator ultrathin Bi_2Se_3 film. *Phys. Rev. B* **82**, 155309 (2010).
45. Marel, van der, D. *In Strongly Correlated Systems*. 269–296 (Springer, Berlin Heidelberg, 2015).
46. Santoso, I. et al. Observation of room-temperature high-energy resonant excitonic effects in graphene. *Phys. Rev. B* **84**, 081403 (2011).
47. LaForge, A. D. et al. Optical characterization of Bi_2Se_3 in a magnetic field: Infrared evidence for magnetoelectric coupling in a topological insulator material. *Phys. Rev. B* **81**, 125120 (2010).
48. Eddrief, M., Vidal, F. & Gallas, B. Optical properties of Bi_2Se_3: from bulk to ultrathin films. *J. Phys. D Appl. Phys.* **49**, 505304 (2016).

49. Eddrief, M., Atkinson, P., Etgens, V. & Jusserand, B. Low-temperature Raman fingerprints for few-quintuple layer topological insulator Bi_2Se_3 films epitaxied on GaAs. *Nanotechnology* **25**, 245701 (2014).
50. Yu, X. J., Diao, C. Z., Venkatesan, T., Breese, M. B. H. & Rusydi, A. A soft x-ray-ultraviolet (SUV) beamline and diffractometer for resonant elastic scattering and ultraviolet-vacuum ultraviolet reflectance at the Singapore synchrotron light source. *Rev. Sci. Instr.* **89**, 113113 (2018).
51. Schmidt, D., You, L., Chi, X., Wang, J. & Rusydi, A. Anisotropic optical properties of rhombohedral and tetragonal thin film $BiFeO_3$ phases. *Phys. Rev. B* **92**, 075310 (2015).
52. Kresse, G. & Hafner, J. Ab initio molecular dynamics for liquid metalS. *Phys. Rev. B* **47**, 558 (1993).
53. Blochl, P. E. Projector augmented-wave method. *Phys. Rev. B* **50**, 17953 (1994).
54. Grimme, S., Ehrlich, S. & Goerigk, L. Effect of the damping function in dispersion corrected density functional theory. *J. Comput. Chem.* **32**, 1456 (2011).
55. Asmara, T. C. et al. Tunable and low-loss correlated plasmons in Mott-like insulating oxides. *Nat. Commun.* **8**, 15271 (2017).
56. Ou, J. Y. et al. Ultraviolet and visible range plasmonics in the topological insulator $Bi_{1.5}Sb_{0.5}Te_{1.8}Se_{1.2}$. *Nat. Commun.* **5**, 5139 (2014).
57. Liou, S. C. et al. Plasmons dispersion and nonvertical interband transitions in single crystal Bi_2Se_3 investigated by electron energy-loss spectroscopy. *Phys. Rev. B* **87**, 085126 (2013).
58. Basov, D. N., Averitt, R. D., van der Marel, D., Dressel, M. & Haule, K. Electrodynamics of correlated electron materials. *Rev. Mod. Phys.* **83**, 471 (2011).
59. Wan, D. Y. et al. Electron transport and visible light absorption in a plasmonic photocatalyst based on strontium niobate. *Nat. Commun.* **8**, 150703 (2017).
60. Pan, Z. H. et al. Measurement of an exceptionally weak electron-phonon coupling on the surface of the topological insulator Bi_2Se_3 using angle-resolved photoemission spectroscopy. *Phys. Rev. Lett.* **108**, 187001 (2012).
61. Woessner, A. et al. Highly confined low-loss plasmons in graphene–boron nitride heterostructures. *Nat. Mater.* **14**, 421 (2015).
62. Stauber, T., Gómez-Santos, G. & Brey, L. Plasmonics in topological insulators: Spin–charge separation, the influence of the inversion layer, and phonon–plasmon coupling. *ACS Photonics* **4**, 2978 (2017).
63. Benia, H. M., Lin, C., Kern, K. & Ast, C. R. Reactive chemical doping of the Bi_2Se_3 topological insulator. *Phys. Rev. Lett.* **107**, 177602 (2011).
64. Bahder, T. B., Tober, R. L. & Bruno, J. D. Pyroelectric effect in semiconductor heterostructures. *Superlattice Microst.* **14**, 149 (1993).
65. Cho, N. I., Poplavko, Y. M. & Noh, S. J. Pyroelectric-like response of III-V semiconductors for microelectronic sensor applications. *J. Korean Phys. Soc.* **42**, 803 (2003).
66. Kim, D. et al. Surface conduction of topological Dirac electrons in bulk insulating Bi_2Se_3. *Nat. Phys.* **8**, 459 (2012).
67. Brahlek, M., Koirala, N., Bansal, N. & Oh, S. Transport properties of topological insulators: Band bending, bulk metal-to-insulator transition, and weak anti-localization. *Solid State Commun.* **215**, 54 (2015).
68. Vidal, F. et al. Photon energy dependence of circular dichroism in angle-resolved photoemission spectroscopy of Bi_2Se_3 Dirac states. *Phys. Rev. B* **88**, 241410 (2013).
69. Veyrat, L. et al. Band bending inversion in Bi_2Se_3 nanostructures. *Nano Lett.* **15**, 7503 (2015).
70. Larson, P. et al. Electronic structure of Bi_2X_3 (X = S, Se, T) compounds: comparison of theoretical calculations with photoemission studies. *Phys. Rev. B* **65**, 085108 (2002).
71. Zhang, W., Yu, R., Zhang, H. J., Dai, X. & Fang, Z. First-principles studies of the three-dimensional strong topological insulators Bi_2Te_3, Bi_2Se_3 and Sb_2Te_3. *N. J. Phys.* **12**, 065013 (2010).
72. Kresse, G. & Hafner, J. Ab initio molecular dynamics for open-shell transition metals. *Phys. Rev. B* **48**, 13115 (1993).
73. Zhu, Z. H. et al. Rashba spin-splitting control at the surface of the topological insulator Bi_2Se_3. *Phys. Rev. Lett.* **107**, 186405 (2011).
74. Park, S. R. et al. Quasiparticle scattering and the protected nature of the topological states in a parent topological insulator Bi_2Se_3. *Phys. Rev. B* **81**, 041405 (2010).